

# Scaling limits of periodic monopoles

Rafael Maldonado\*

*Department of Mathematical Sciences,  
South Road, Durham DH1 3LE, UK*

February 26, 2022

## Abstract

The purpose of this note is to explore the structure of singly periodic monopoles for different values of the size to period ratio. The transition between a chain of small monopoles and the approximately two dimensional chain of large monopoles takes us through a region with an unintuitive dependence on the periodic direction. The focus is mainly on the smooth  $SU(2)$  monopole of charge 2.

## 1 Introduction

Periodic monopoles have been studied in the past by means of the generalised Nahm transform. In [1], it was shown that the Bogomolny (monopole) equations on  $\mathbb{R}^2 \times S^1$  with coordinates  $\zeta = x + iy$  and  $z \sim z + \beta$  are mapped to solutions of Hitchin equations

$$F_{s\bar{s}} = -\frac{1}{4}[\Phi, \Phi^\dagger] \quad D_{\bar{s}}\Phi = 0$$

on a cylinder described by  $(r, t) \in \mathbb{R} \times S^1$ , with  $s = r + it$ . We will work with the notation of [2], in which a class of solutions to the Hitchin equations corresponding to a chain of charge 2 is

$$\Phi = \begin{pmatrix} 0 & \mu_+ e^{\psi/2} \\ \mu_- e^{-\psi/2} & 0 \end{pmatrix} \quad A_{\bar{s}} = a\sigma_3 \quad A_s = -\bar{a}\sigma_3$$

where the characteristic equation of  $\Phi$  is fixed by the spectral curve as described in [1],<sup>1</sup>

$$-\det(\Phi) = \mu_+ \mu_- = C \cosh(\beta s) + K/2$$

and  $a$  and  $\psi$  are functions of  $(r, t)$  satisfying  $4a = -\partial_{\bar{s}}\psi$ ,

$$\nabla^2 \text{Re}(\psi) = 2 \left( |\mu_+|^2 e^{\text{Re}(\psi)} - |\mu_-|^2 e^{-\text{Re}(\psi)} \right) \quad (1)$$

---

\*[rafael.maldonado@durham.ac.uk](mailto:rafael.maldonado@durham.ac.uk)

<sup>1</sup>Here we follow the conventions of [2, 3] for the sign of  $K$ . The opposite sign was used in [4], the only difference being a rotation of the monopole system by  $\pi/2$  about the  $z$  axis.

with  $\text{Im}(\psi)$  chosen in such a way that  $\Phi$  has the correct  $t$ -period.

The inverse Nahm operator

$$\Delta\Psi = \begin{pmatrix} \mathbf{1}_2 \otimes (2\partial_{\bar{s}} - z) + 2A_{\bar{s}} & \mathbf{1}_2 \otimes \zeta - \Phi \\ \mathbf{1}_2 \otimes \bar{\zeta} - \Phi^\dagger & \mathbf{1}_2 \otimes (2\partial_s + z) + 2A_s \end{pmatrix} \Psi = 0 \quad (2)$$

with solutions normalised to

$$\int_{-\infty}^{\infty} dr \int_{-\pi/\beta}^{\pi/\beta} dt (\Psi^\dagger \Psi) = \mathbf{1}_2$$

then allows a numerical construction of the monopole fields

$$\hat{\Phi} = i \int_{-\infty}^{\infty} dr \int_{-\pi/\beta}^{\pi/\beta} dt (r \Psi^\dagger \Psi) \quad \hat{A}_i = \int_{-\infty}^{\infty} dr \int_{-\pi/\beta}^{\pi/\beta} dt (\Psi^\dagger \partial_i \Psi)$$

and an analytical study of their symmetries.

We will focus on the two classes of solution with  $\alpha = 0$ , [3], for which the zeros of  $\det(\Phi)$  are placed either in the same or different entries of  $\Phi$ :

- The ‘zeros together’ solution has  $\text{Im}(\psi) = 0$  and

$$\mu_+ = C \cosh(\beta s) + K/2 \quad \mu_- = 1.$$

- The ‘zeros apart’ solution has  $\text{Im}(\psi) = -\beta t$  and

$$\mu_{\pm} = \sqrt{C/2} \left( e^{\beta s/2} + W^{\pm 1} e^{-\beta s/2} \right) \quad \text{where} \quad K/C = W + W^{-1}. \quad (3)$$

The choice of solution affects the symmetries and scattering processes of the corresponding monopoles, as will be discussed in section 2.

In the monopole picture, these solutions correspond, for the complex modulus  $|K| \gg 2C$ , to monopoles located approximately at  $\zeta = \pm \sqrt{K/2}$  and with zero  $z$ -offset, [3]. The positive real parameter  $C$  determines the size to period ratio of the constituent monopoles. Periodic monopoles have also been observed to split into two constituent energy peaks, in this case separated by  $|C\sqrt{2/K}|$  when  $|K| \gg 2C$ .<sup>2</sup> The aim of this paper is to study how the monopole shape and location depend on  $K$  and  $C$ .

Periodic monopoles of charge 1 and 2 were constructed in [6] and [2]. In [3], the ‘spectral approximation’ was introduced, allowing the monopole fields to be read off from the spectral curve when  $C$  is large. This paper gives further evidence on the validity of this approximation and illustrates how it arises from the well separated monopoles at small  $C$ . The effect of  $C$  on the moduli space of solutions was discussed further in [4].

This paper is arranged as follows. In section 2 the symmetries of charge 2 periodic monopoles are given. The limits of small and large  $C$  are discussed in sections 3 and 4. The intermediate regime is then studied in section 5, and some comments on the generalisation to higher charges are made in section 6.

---

<sup>2</sup>Such behaviour has been extensively researched for periodic instantons, which have monopole constituents [5]. The case of periodic monopoles displays an important difference with the caloron case, in that constituents are always present due to the asymptotic holonomy always being non-trivial [3], although their separation reduces as  $C \rightarrow 0$ . Furthermore, it is not yet clear whether there is in this case a meaningful description of the constituents as separate entities in their own right.

## 2 Monopole symmetries

Spatial symmetries of the monopole can be deduced from the structure of the inverse Nahm operator (2) as follows. The symmetries of the spectral curve motivate a transformation of the coordinates on the Hitchin cylinder, such that the transformed Nahm/Hitchin fields can be expressed in terms of a gauge transformation of the original fields. A suitable transformation of the spatial  $(\zeta, z)$  coordinates which twist the inverse Nahm operator leaves its kernel unchanged, implying the monopole fields at the transformed spatial coordinates are gauge equivalent to the original monopole fields. This procedure was discussed in [2] and extended in [3], and the reader is referred to these for a detailed discussion. This section summarises the symmetries relevant to the charge 2 periodic monopole, extending those presented in [3] by considering more carefully the branching structure of the solutions for  $|K| \leq 2C$ .

In the ‘zeros together’ case the monopole fields display the spatial symmetries  $(\zeta, z) \sim (\bar{\zeta}, -z)$  for  $K \in \mathbb{R}$ , and  $(\zeta, z) \sim (i\bar{\zeta}, -z)$  for  $K \in i\mathbb{R}$ . In both cases  $(\zeta, z; K) \sim (i\zeta, z; -K)$ , such that when  $K = 0$  there is an enhanced  $C_4$  symmetry  $(\zeta, z) \sim (i\zeta, z)$ .

The ‘zeros apart’ case enjoys the symmetry  $(\zeta, z) \sim (\bar{\zeta}, -z)$  for  $W \in \mathbb{R}$  and  $(\zeta, z) \sim (i\bar{\zeta}, -z)$  for  $W \in i\mathbb{R}$ , in both cases with  $(\zeta, z, W) \sim (\bar{\zeta}, \beta/2 - z, \bar{W}^{-1})$  relating the incoming and outgoing legs of the geodesics on the half-lines  $W = p^2$  and  $W = ip^2$  for  $p > 0$ . There are two cases with enhanced symmetry, which will be of particular interest in this paper:

- for  $W = 1$ ,  $(\zeta, z) \sim (\zeta, \beta/2 - z) \sim (\zeta, z + \beta/2)$ ,
- for  $W = i$ ,  $(\zeta, z) \sim (i\zeta, \beta/2 - z) \sim (i\zeta, z + \beta/2)$ .

These symmetries involve a chain in the sign of  $\hat{\Phi}$ , but correctly describe symmetries of the energy density. Unlike for the charge 2 monopole in  $\mathbb{R}^3$ , the symmetries are always discrete due to the splitting into constituents. As  $|C|$  is reduced, the constituents move closer together and in the limit  $C \rightarrow 0$  the phase of  $C$  can have no effect, reproducing the axially symmetric charge 2 monopole [7] in this limit.

## 3 Small C

In the limit of small size to period ratio monopole chains behave like monopoles in  $\mathbb{R}^3$ , whose energy density peaks roughly at the location of the zeros of the Higgs field. The two scattering processes identified in section 2 correspond in this limit to the Atiyah-Hitchin rounded cone (‘zeros together’) and trumpet (‘zeros apart’), as geodesic sub-manifolds of the full four dimensional moduli space, [4]. Although it is straightforward to reach the above conclusions numerically, the limit is nevertheless delicate to provide analytically in the present formulation. In particular, it is not clear how the ALG type metric reduces to the usual ALF of monopoles in  $\mathbb{R}^3$  [8]. In this limit we also see that the coordinate  $W$  goes bad, in the sense that the value of  $W$  at which the monopole Higgs zeros coincide increases as  $C \rightarrow 0$ , as shown in figure 1.

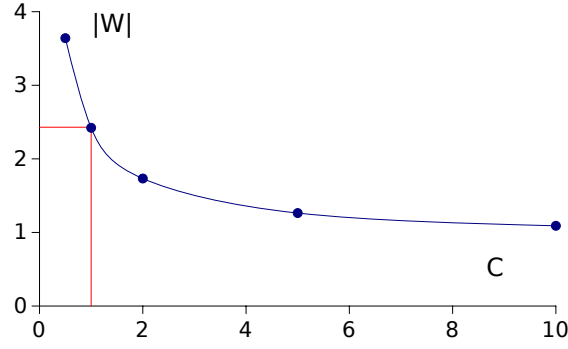


Figure 1:  $|W|$  against  $C$ , showing how the value of  $|W|$  at which the monopole Higgs zeros coincide in the ‘zeros apart’ configuration depends on  $C$ , both for  $W \in \mathbb{R}$  and  $W \in i\mathbb{R}$ . For ‘zeros together’, the monopole zeros always coincide when  $K = 0$ .

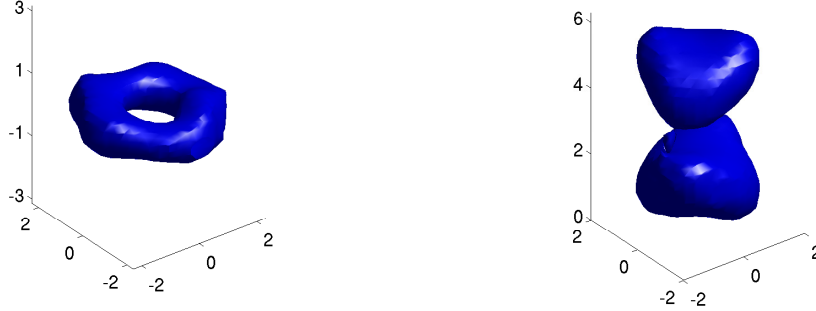


Figure 2: Energy density for charge 2 monopole in the ‘zeros together’ (left) and ‘zeros apart’ (right) configuration with  $C = 1$  and  $W = i$ .

The particularly symmetric case with  $K = 0$  is shown in figure 2 for the ‘zeros together’ and ‘zeros apart’ solutions, displaying the expected spatial symmetries (section 2 and ref. [3]). The ‘zeros apart’ geodesic for  $C = 1$  and  $W > 1$  has two monopole chains incoming along the  $x$  axis, whose energy density is peaked at the Higgs zeros. At  $W \approx 2.43$  (figure 1) the Higgs zeros coincide to give a toroidal configuration (figure 3 left). Reducing  $K$  further, the ring breaks up along the  $z$  axis, giving two copies of a charge 1 monopole when  $W = 1$  (figure 3 right, see also [2, 9]), which move apart parallel to the  $x$  axis for  $W < 1$ . The geodesic with  $W \in i\mathbb{R}$  again involves a double scattering, though this time the ‘doubled’ charge 1 chain is not encountered and chains depart at  $90^\circ$  to the incoming chains.

### 3.1 Regaining the Nahm equations

Defining the combinations  $\Phi = i(T_1 + iT_2)$ ,  $A_r = T_0$ ,  $A_t = T_3$  of the Hitchin fields with  $T_i = \frac{1}{2}if_i\sigma_i$ , we take the limit  $C = 0$ , such that  $\det(\Phi) = -K/2$  and the Hitchin fields

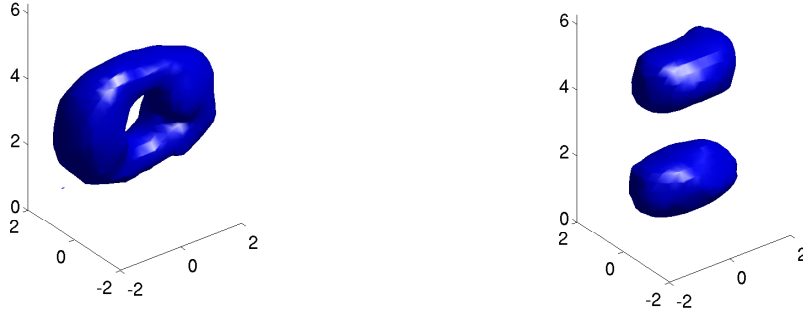


Figure 3: Energy density for charge 2 monopole in the ‘zeros apart’ configuration with  $C = 1$  and  $W = 2.43$  (left) and  $W = 1$  (right).

on the cylinder depend only on  $r$ . This reproduces the usual Nahm equations in  $\mathbb{R}^3$ , and although this approach is only valid in the strict limit  $C \rightarrow 0$ , it is interesting to note how the different ‘zeros together’ and ‘zeros apart’ solutions can still be seen in this limit.

In the above notation, the Hitchin equations become Nahm equations, such that the functions  $f_i$  satisfy

$$\frac{df_i}{dr} = \frac{1}{2} \epsilon_{ijk} f_j f_k \quad (4)$$

and the Hitchin fields become

$$\Phi = -\frac{1}{2} \begin{pmatrix} 0 & f_1 + f_2 \\ f_1 - f_2 & 0 \end{pmatrix} \quad \frac{d\psi}{dr} = 2f_3$$

where we have chosen a gauge with  $A_r = 0$ . The spectral curve tells us that

$$-\det(\Phi) = \frac{1}{4}(f_1^2 - f_2^2) = C \cosh(\beta s) + K/2,$$

and (4) immediately requires  $C = 0$ . In this form, with  $\alpha = 0$  and  $K \in \mathbb{R}$ , the Nahm equations can easily be solved in terms of elliptic functions [10, 7].

For real  $f_i$  the Nahm transform provides a clear link between the symmetries of  $(\zeta, z)$  and those of  $(\Phi, T_3)$ . It is thus expected that there will be different solutions to the Nahm equations corresponding to the relative magnitudes of  $f_1^2, f_2^2, f_3^2$ . We note from [10, 7] that for large  $K$  the monopoles are localised along the axis  $e_i$  corresponding to the largest of the  $f_i^2$ . We will fix  $\zeta = e_1 + ie_2$  and  $z = e_3$  (this is a gauge choice on the Nahm data), with monopoles incoming along  $e_1$ .

First of all we take  $f_1^2 \geq f_2^2 \geq f_3^2$ , and define a function  $a(K)$  and the elliptic modulus  $k \in [0, 1]$  by

$$f_1^2 - f_2^2 = 2K \quad f_1^2 - f_3^2 = a^2 \quad 2K = a^2 k^2$$

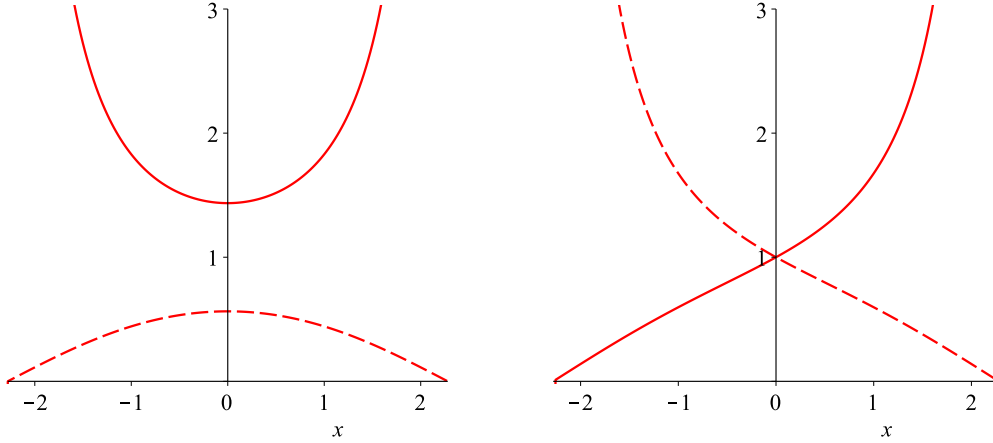


Figure 4:  $(f_1 + f_2)/a$  (solid) and  $(f_1 - f_2)/a$  (dashed) for  $k = 0.9$  plotted against  $x = ar$  (left, for  $f_1^2 > f_2^2 > f_3^2$ ) and  $x = \sqrt{2K}r$  (right, for  $f_1^2 > f_3^2 > f_2^2$ ).

which are solved in terms of Jacobi elliptic functions defined for  $|ar| < \mathbf{K}(k)$ ,

$$f_1 = \text{adc}_k(ar) \quad f_2 = ak' \text{nc}_k(ar) \quad f_3 = ak' \text{sc}_k(ar).$$

In the limit  $K \rightarrow 0$  the monopole chains approach one another and<sup>3</sup>

$$f_1 = f_2 = a \sec(ar) \quad f_3 = a \tan(ar) \quad \psi = 2 \log(2ab \sec(ar))$$

for some constant  $b$ .

The equality  $f_1 = f_2$  in this limit describes a monopole configuration which is axially symmetric about the periodic axis, and leads to  $90^\circ$  scattering in the plane when  $K$  becomes negative (when  $f_2^2 \geq f_1^2 \geq f_3^2$ ).

Fig. 4 (left) shows a plot of  $f_1 \pm f_2$  for  $k = 0.9$ , illustrating how both zeros are in the same component of  $\Phi$  (i.e. the ‘zeros together’ solution).

On the other hand, there is the possibility of having  $f_1^2 \geq f_3^2 \geq f_2^2$ . This time,

$$f_1^2 - f_2^2 = 2K \quad f_1^2 - f_3^2 = a^2 \quad 2Kk^2 = a^2$$

and the solution is

$$f_1 = \sqrt{2K} \text{dc}_k(\sqrt{2K}r), \quad f_2 = \sqrt{2K}k' \text{sc}_k(\sqrt{2K}r), \quad f_3 = \sqrt{2K}k' \text{nc}_k(\sqrt{2K}r).$$

<sup>3</sup>This expression for  $\psi$  can also be obtained from the ‘zeros together’ Hitchin equations with  $K = 0$  by use of an approximate solution [11] which improves as  $\beta \rightarrow \infty$ . This approach clarifies the transition, as  $\beta$  is increased, between the smooth Nahm/Hitchin data valid on the entire length of the cylinder and the solution valid on the finite interval  $ar \in \pi/2(-1, 1)$  with singularities at the endpoints (note that  $\mathbf{K}(0) = \pi/2$ ). In essence, the singular solution for  $\psi$  arises from the  $\beta \rightarrow \infty$  limit of the boundary conditions  $\psi \sim \pm \beta r$  for  $r \rightarrow \pm \infty$ . It is pleasing to see that the limits  $\beta \rightarrow \infty$  and  $C \rightarrow 0$  yield the same result, in both cases describing chains of small monopoles.

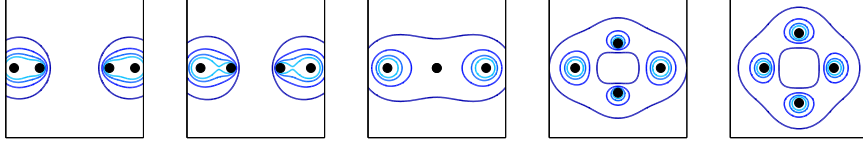


Figure 5: Sequence (to be read from left to right and top to bottom) showing the scattering of monopole chains with  $K \in \mathbb{R}$  within the spectral approximation.

This time, when  $K = 0$  we simply have  $f_1 = f_2 = f_3 = 0$ , which is the Nahm data for a single monopole. Fig. 4 (right) shows  $f_1 \pm f_2$ . The zeros of  $\Phi$  are now in different components and scattering is consistent with the ‘zeros apart’ solution.

## 4 Large $C$

In the opposite limit, of large monopole size to period ratio, the structure again simplifies. As  $C$  is increased, the fields become increasingly independent of  $z$  and the spectral approximation [3] becomes an accurate description of the monopole. The monopole Higgs field is known explicitly in this limit and can be read off directly from the spectral curve,

$$\hat{\Phi} = \frac{i}{\beta} \operatorname{Re} \left( \cosh^{-1} \left( \frac{2\zeta^2 - K}{2C} \right) \right) \sigma_3,$$

and the energy density calculated through

$$\mathcal{E} = \frac{1}{4} \nabla^2 |\operatorname{tr}(\hat{\Phi}^2)|. \quad (5)$$

Geodesic motion with  $K \in \mathbb{R}$  describes the movement of four lumps of energy density located at  $\zeta = \pm\sqrt{K/2} \pm C$  undergoing a double scattering via a cross-shaped configuration at  $K = 0$ , as shown in figure 5.

In the large  $C$  limit there is also a simplification in the solutions of the Hitchin equations. The  $C$  dependence of  $\mu_{\pm}$  in (1) means a non-trivial solution for  $\nabla^2 \operatorname{Re}(\psi)$  is only supported at small  $C$  and in the vicinity of the two regions  $\mu_{\pm} \approx 0$ . Thus, in the large  $C$  limit, the smooth solution to (1) approaches the singular solution obtained by setting both sides to zero.

Details of the geometry of the moduli space in this limit are given in [3, 4]. The solutions to the Nahm/Hitchin equations in this limit, referred to above, imply that the metric obtained from this data depends only on  $\det(\Phi)$ , and is hence the same for the ‘zeros together’ and ‘zeros apart’ solutions. This is identical to the metric found from the spectral approximation to the monopole fields in [3]. This metric has two logarithmic singularities on the  $K$  plane. Numerically, for  $C \gtrsim 36$  we recover the  $z$ -independent fields as approximately cylindrical tubes of energy density aligned with the  $z$  axis.

#### 4.1 Nahm transform for large $C$

The large scale limit allows a demonstration of an example of the Nahm transform for the construction of solutions to the Hitchin equations on  $\mathbb{R}^2$  (twice dimensionally reduced self-dual Yang-Mills equations). The general theory of Nahm transforms [12] suggests that the Nahm transform on  $\mathbb{R}^2$  is ‘self-reciprocal’ [13], thus mapping the large  $C$  limit of the periodic monopole to Hitchin equations on  $\mathbb{R}^2$ , with a different topology and boundary conditions. It is not clear how to ‘unwrap’ the Hitchin cylinder in this limit, or how one might deal with the singular nature of the solutions. However, as a step towards understanding this instance of the Nahm transform, we show that in this limit the ‘spectral approximation’ can also be applied to the forward Nahm transform, allowing us to reproduce the initial Nahm data from the approximate monopole fields. Below we look specifically at the charge 1 periodic monopole, although the argument can equally be applied to higher charges.

The inverse Nahm operator for the charge 1 periodic monopole [6] is

$$\Delta\Psi = \begin{pmatrix} 2\partial_{\bar{s}} - z & \zeta - \Phi \\ \bar{\zeta} - \Phi^\dagger & 2\partial_s + z \end{pmatrix} \begin{pmatrix} \psi_{11} & \psi_{12} \\ \psi_{21} & \psi_{22} \end{pmatrix} = 0, \quad (6)$$

where  $\Phi = C \cosh(\beta s)$ . To study the large  $C$  limit, we suppress  $z$  dependence (setting  $z = 0$  above) and define new fields

$$i \int_{\mathbb{R}^2} dr dt (s \Psi^\dagger \Psi) = i\hat{\phi} \quad \int_{\mathbb{R}^2} dr dt (\Psi^\dagger \partial_j \Psi) = \hat{a}_j$$

where  $i\hat{\phi} = \hat{\Phi} - i\hat{A}_z$  and  $j = x, y$ . These fields satisfy Hitchin equations in  $\mathbb{R}^2$ . Equation (6) has an approximate solution valid at large  $C$ , [6, 3], in which the columns of  $\Psi$  are Gaussian peaks at  $s = \pm s_0$  with  $s_0(\zeta)$  defined through  $C \cosh(\beta s_0) = \zeta$ . In this limit the monopole fields are  $\hat{\phi} = s_0 \sigma_3$ ,  $\hat{a} = 0$ .

The idea is to use these approximate monopole fields to explicitly perform the forward Nahm transform, i.e. starting from  $\hat{\phi}, \hat{a}$  obtain  $\Phi$  and  $A$ . The Nahm operator is

$$\hat{\Delta}\hat{\Psi} = \begin{pmatrix} 2\partial_{\bar{\zeta}} & 0 & s - s_0 & 0 \\ 0 & 2\partial_{\bar{\zeta}} & 0 & s + s_0 \\ \bar{s} - \bar{s}_0 & 0 & 2\partial_{\zeta} & 0 \\ 0 & \bar{s} + \bar{s}_0 & 0 & 2\partial_{\zeta} \end{pmatrix} \begin{pmatrix} \hat{\psi}_1 \\ \hat{\psi}_2 \\ \hat{\psi}_3 \\ \hat{\psi}_4 \end{pmatrix} = 0, \quad (7)$$

normalised solutions to which should give the charge 1 Nahm/Hitchin data,

$$\Phi = \int_{\mathbb{R}^2} dx dy \zeta \sum_{i=1}^4 |\hat{\psi}_i|^2 = C \cosh(\beta s) \quad A = \int_{\mathbb{R}^2} dx dy \sum_{i=1}^4 \bar{\hat{\psi}}_i \partial_j \hat{\psi}_i = 0.$$

Solutions to the forward Nahm operator (7) are found using the same ideas as those for the inverse transform. First of all, we note that the equations for  $\hat{\psi}_1$  and  $\hat{\psi}_3$  decouple



from those for  $\hat{\psi}_2$  and  $\hat{\psi}_4$ . Writing  $\zeta_0 = C \cosh(\beta s)$  and  $\zeta = \zeta_0 + \delta$ , we have

$$s - s_0 = \frac{1}{\beta} \cosh^{-1} \left( \frac{\zeta_0}{C} \right) - \frac{1}{\beta} \cosh^{-1} \left( \frac{\zeta_0 + \delta}{C} \right) = -\frac{\zeta - \zeta_0}{\beta} \xi + \mathcal{O}(\delta^2)$$

where  $\xi^{-1} = C \sinh(\beta s)$ .  $\hat{\psi}_1$  and  $\hat{\psi}_3$  are supported away from  $s = 0$ , and we make the Ansatz  $\hat{\psi}_{1,3} \sim \exp(-c|\zeta - \zeta_0|^2)$ , resulting in  $c = |\xi|/(2\beta)$  and  $\hat{\psi}_3 = -\xi^{-1/2} \bar{\xi}^{1/2} \hat{\psi}_1$ .

The important point now is that, if we remain on the correct branch of  $\cosh^{-1}$ , the quantity  $(s + s_0)$  will never be close to zero (as in [6], we must avoid the points  $\zeta_0 = \pm C$ ). Thus,  $\hat{\psi}_{2,4}$  are small and slowly varying compared to  $\hat{\psi}_{1,3}$ . We thus approximate  $\hat{\psi}_{2,4} \approx 0$ , so that normalising gives

$$|\hat{\psi}_{1,3}|^2 = \frac{|\xi|}{2\pi\beta} e^{-|\xi||\zeta - \zeta_0|^2/\beta}.$$

The consistency relation  $\hat{\psi}_3 = \pm \bar{\hat{\psi}}_1$  fixes the phases on  $\hat{\psi}_{1,3}$ ,

$$\hat{\psi}_1 = - \left( \frac{\xi}{2\pi\beta} \right)^{1/2} e^{-|\xi||\zeta - \zeta_0|^2/(2\beta)}, \quad \hat{\psi}_3 = \left( \frac{\bar{\xi}}{2\pi\beta} \right)^{1/2} e^{-|\xi||\zeta - \zeta_0|^2/(2\beta)}, \quad (8)$$

yielding the expected Hitchin fields,  $\Phi = \zeta_0 = C \cosh(\beta s)$ ,  $A = 0$ . Note the solution (8) is again exponentially localised, and the scaling with  $\beta$  in opposite to that of  $\Psi$ .

## 5 Intermediate C

Now the small and large  $C$  limits have been established, our aim is to understand the intermediate regime. Here we focus on the ‘zeros apart’ case, which displays a rich  $z$  behaviour. It is instructive to study the geodesics  $W \in \mathbb{R}$ ,  $W \in i\mathbb{R}$  and  $|W| = 1$ .

For  $W = i$ , the transition from small to large  $C$  involves the resolution of the energy lumps of figure 2 into two constituents each. Curiously, however, the constituents are not aligned with the  $x$  and  $y$  axes but with the lines  $x \pm y = 0$ , such that the chain has been twisted by different amounts along its length, figure 6. The  $W = i$  configuration on the  $W \in i\mathbb{R}$  geodesic is an intermediate case between  $W = ip$  with  $p \gg 1$  (for small  $C$ , this describes incoming chains along  $x = y$  at  $z = \beta/2$ ) and  $0 < p \ll 1$  (outgoing chains along  $x = -y$  at  $z = 0$ ). Figure 7 shows configurations with  $W = 2i$  and  $W = 1.125i$  for  $C = 2$ , illustrating the fusing of two chains in the  $W \in i\mathbb{R}$  geodesic and showing the transition between the  $W = i$  chains of figures 2 and 6.

The  $W = 1$  configuration is the midpoint of scattering via the  $W \in \mathbb{R}$  geodesic, for which outgoing chains are simply shifted by  $\beta/2$  relative to the ingoing chains (figure 8 left).

We now describe the  $|W| = 1$  geodesic. When  $W = 1$ , we have a ‘chain of doughnuts’, all equally aligned and with period  $\beta/2$ . Altering the phase of  $W$ , the portion of the chain in the vicinity of  $z = \beta/2$  rotates anticlockwise while that near  $z = 0$  and  $z = \beta$  rotates clockwise such that at  $W = i$  they are at  $45^\circ$  to the coordinate axes. These configurations are shown in figures 6 and 8 for  $C = 4$ .

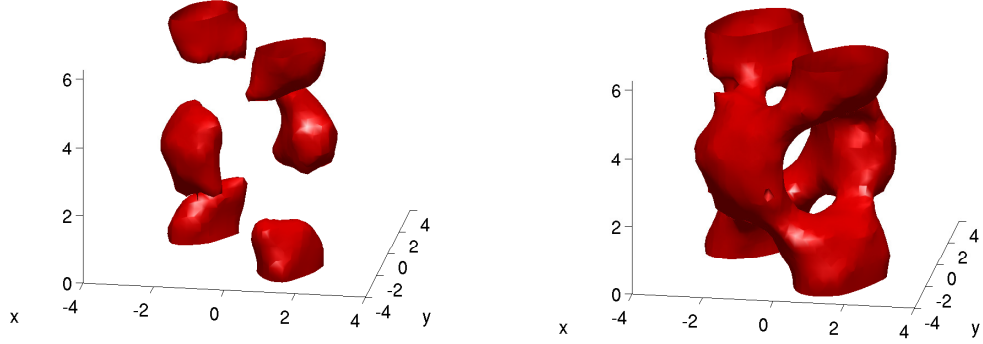


Figure 6: Energy density isosurfaces for  $C = 4$ ,  $W = i$ . On the left we see the constituent structure, and on the right the twisted chain. Note the similarity to the Skyrmion chain configurations obtained in [14].

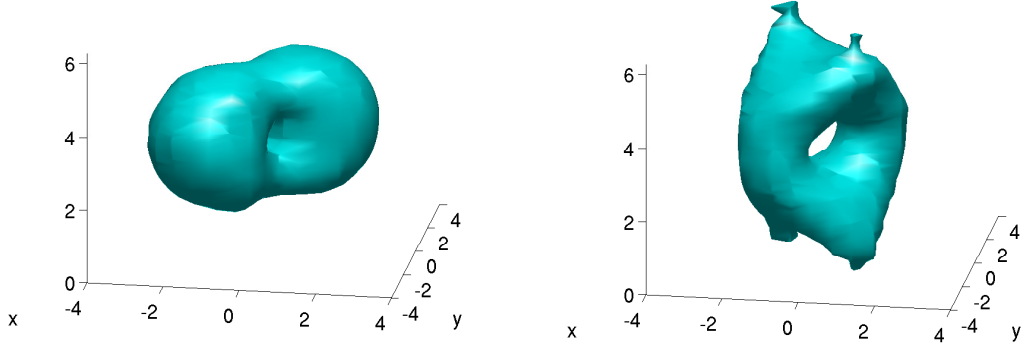


Figure 7: Two points on the  $W = i$  geodesic with  $C = 2$ . Left:  $W = 2i$ , right:  $W = 1.125i$ . As well as illustrating the scattering process, these energy density plots show how there is a transition between the  $C = 1$  case, where the energy is peaked in two regions near the  $z$  axis, and the  $C = 4$  case, in which the energy is peaked away from the  $z$  axis. The ‘four pronged’ structures of figure 2 can be visualised as splitting the right hand structure above along  $z = \pi$ .

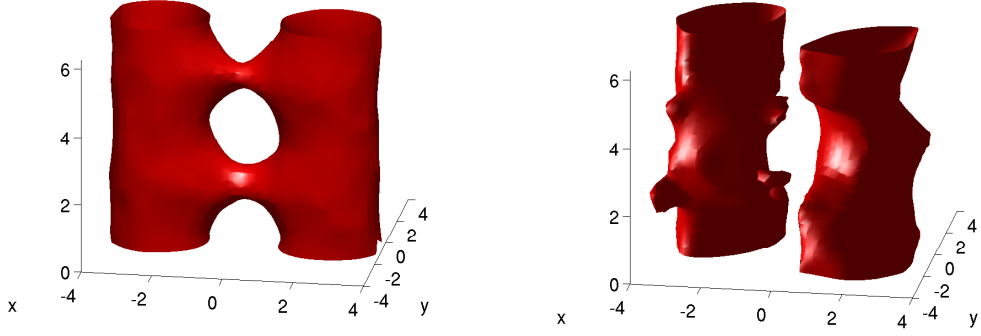


Figure 8: Scattering for  $C = 4$ . Left:  $W = 1$ , right:  $W = e^{i\pi/3}$ . The  $W = i$  configuration is shown in figure 6.

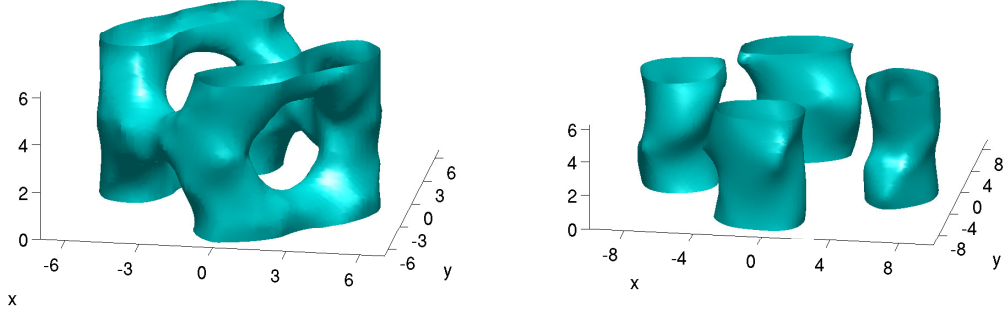


Figure 9: Left:  $C = 16$ ,  $W = i$ , right:  $C = 36$ ,  $W = i$ . Note how we approach the  $z$ -independent result of the spectral approximation (figure 5, middle panel).

As  $C$  is increased, the configuration deforms as shown in figure 9. The energy lumps stretch in the  $xy$  plane and fuse along  $z$  such that when  $C$  is large enough, there are tubes of energy density located in a cross shape aligned with the  $x$  and  $y$  axes.

Even for intermediate values of  $C$ , one can make a link with the results of the spectral approximation by integrating the energy density along a  $z$  period across the  $xy$  plane. The resulting quantity, shown in figure 10, is found to resemble the energy density expected from the spectral approximation, insofar as the peaks are located along the coordinate axes and there is still a minimum at  $x = y = 0$ .

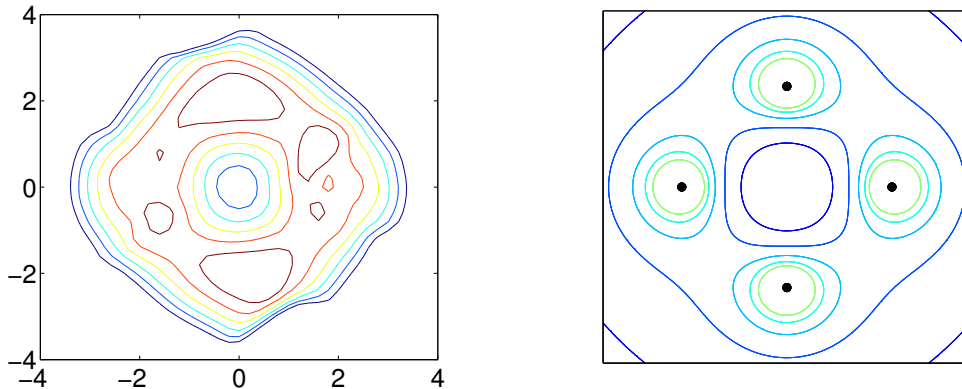


Figure 10: Left: energy density integrated along a period for  $C = 4$ ,  $K = 0$ . Unlike in fig. 6 the energy peaks here are at the locations expected from the spectral approximation (right). Note that this comparison requires a rescaling of the  $x, y$  coordinates by a factor of  $\sqrt{C}$ .

## 6 Higher charge chains

In this section we briefly make mention of the limits of varying  $C$  with the charge 3 periodic monopole described in [9]. For  $K = 0$  and small  $C$  the charge 3 configuration consists of an approximately toroidal charge 2 monopole at  $z = \beta/6$  and a roughly spherical charge 1 monopole at  $z = 2\beta/3$ . For large  $C$ , the spectral approximation predicts a collection of tubes in a hexagonal configuration, with two of them found on the  $x$  axis.

A numerical study of the effect of increasing  $C$  is hindered by the need to make an appropriate choice of step size in performing the numerical derivative of  $\hat{\Phi}$  to obtain the energy density via (5), as  $\hat{\Phi}$  changes rapidly over small distances. Nonetheless, the charge 2 results suggest that for intermediate values of  $C$  the configuration can be thought of as a chain of tetrahedra in alternating orientations disposed of as follows: place a base of the tetrahedron at  $z = \beta/6$ , oriented such that one of the vertices is aligned with the  $y$  axis and another vertex is on the  $z$  axis at  $z = 2\beta/3$ . The next tetrahedron shares the base, but is ‘upside down’ (with a vertex at  $z = -\beta/3$ ) and rotated around the  $z$  axis by  $\pi/3$  relative to the first.

One can understand higher charges in a similar way. For instance, the charge 4 configuration can occur in one of two types: either a chain of square pyramids disposed as with the tetrahedra of the charge 3 chain (this is the ‘zeros apart’ configuration of [9]), or as a chain of cubes, each rotated by  $\pi/4$  relative to the last (this is the ‘zeros opposite’ configuration).

## References

- [1] S. Cherkis, A. Kapustin, *Nahm Transform for Periodic Monopoles and  $N=2$  Super Yang-Mills Theory*, Commun. Math. Phys. **218** (2001) 333, [arXiv:hep-th/0006050](#)
- [2] D. Harland, R. S. Ward, *Dynamics of periodic monopoles*, Phys. Lett. **B 675** (2009) 262, [arXiv:0901.4428 \[hep-th\]](#)
- [3] R. Maldonado, *Periodic monopoles from spectral curves*, JHEP02(2013)099, [arXiv:1212.4481 \[hep-th\]](#)
- [4] R. Maldonado, R. S. Ward, *Geometry of periodic monopoles*, Phys. Rev. **D 88** (2013) 125013, [arXiv:1309.7013 \[hep-th\]](#)
- [5] K. Lee, C. Lu,  *$SU(2)$  calorons and magnetic monopoles*, Phys. Rev. **D 58** (1998) 025011
- [6] R.S. Ward, *Periodic monopoles*, Phys. Lett. **B 619** (2005) 177, [arXiv:hep-th/0505254](#)
- [7] N. Manton, P. Sutcliffe, *Topological Solitons*, CUP (2007)
- [8] S. A. Cherkis, A. Kapustin, *Hyper-Kähler metrics from periodic monopoles*, Phys. Rev. **D 65** (2002) 084015, [arXiv:hep-th/0109141](#)
- [9] R. Maldonado, *Higher charge periodic monopoles*, [arXiv:1311.6354 \[hep-th\]](#)
- [10] S. A. Brown, H. Panagopoulos, M. K. Prasad, *Two separated  $SU(2)$  Yang-Mills-Higgs monopoles in the Atiyah-Drinfeld-Hitchin-Manin-Nahm construction*, Phys. Rev. **D 26** (1982) 854
- [11] D. Harland, private communication
- [12] M. Jardim, *A survey on Nahm transform*, J. Geom. Phys. **52** (2004) 313, [arXiv:math/0309305 \[math.DG\]](#)
- [13] E. Corrigan, P. Goddard, *Construction of Instanton and Monopole Solutions and Reciprocity*, Ann. Phys. **154**, 253-279 (1984)
- [14] D. Harland, R. S. Ward, *Chains of skyrmions*, JHEP12(2008)093, [arXiv:0807.3870 \[hep-th\]](#)